

# Warm Molecular Gas Traced with CO $J = 7 \rightarrow 6$ in the Galaxy's Central 2 pc: Dynamical Heating of the Circumnuclear Disk

C. M. Bradford<sup>1</sup>, G. J. Stacey, T. Nikola

*Department of Astronomy, Cornell University, Ithaca, NY 14853*

A. D. Bolatto

*Department of Astronomy and Radio Astronomy Laboratory, University of California, Berkeley, CA 94720-3411*

J.M. Jackson

*Institute for Astrophysical Research, Boston University, Boston, MA 02215*

and

M. L. Savage, J. A. Davidson

*USRA SOFIA, NASA Ames Research Center, Moffet Field, CA 94035*

## ABSTRACT

We present an 11'' resolution map of the central two parsecs of the Galaxy in the CO  $J=7 \rightarrow 6$  rotational transition. The CO emission shows rotation about Sgr A\*, but also evidence for non-circular turbulent motion and a clumpy morphology. We combine our dataset with available CO measurements to model the physical conditions in the disk. We find that the molecular gas in the region is both warm and dense, with  $T \sim 200\text{--}300$  K,  $n_{\text{H}_2} \sim 5\text{--}7 \times 10^4 \text{ cm}^{-3}$ . The mass of warm molecular gas we measure in the central two parsecs is at least  $2000 M_{\odot}$ , about 20 times the UV-excited atomic gas mass, ruling out an UV heating scenario for the molecular material. We compare the available spectral tracers with theoretical models and conclude that molecular gas is heated with magneto-hydrodynamic shocks with  $v \sim 10\text{--}20 \text{ km s}^{-1}$  and  $B \sim 0.3\text{--}0.5 \text{ mG}$ . Using the conditions derived with the CO analysis, we include the other important coolants – neutral oxygen and molecular hydrogen – to estimate the total cooling budget of the molecular material. We derive a mass to luminosity ratio of

---

<sup>1</sup>present address: Jet Propulsion Laboratory, Mail Stop 169-507, Pasadena, CA, 91109, Matt.Bradford@jpl.nasa.gov

$\sim 2\text{--}3 M_{\odot} / L_{\odot}$ , which is consistent with the total power dissipated via turbulent decay in 0.1 pc cells with  $v_{\text{rms}} \sim 15 \text{ km s}^{-1}$ . These size and velocity scales are comparable to the observed clumping scale and the velocity dispersion. At this rate, the material near Sgr A\* is dissipating its orbital energy on an orbital timescale, and cannot last for more than a few orbits. Our conclusions support a scenario in which the features near Sgr A\* such as the CND and northern arm are generated by infalling clouds with low specific angular momentum.

*Subject headings:* Galaxy: center — Galaxy: nucleus – ISM: molecules – turbulence

## 1. Introduction

The Galactic Center provides the opportunity to study many of the fascinating phenomena associated with massive black holes and galactic nuclei in the greatest detail. The region is likely similar to the nuclei of galaxies beyond the Milky Way, particularly those harboring low-luminosity AGN (LLAGN) with similar sub-Eddington luminosities. Since the Galactic Center radio and infrared sources were first discovered decades ago (Oort & Rougoor 1960; Becklin & Neugebauer 1968, 1969; Balick & Brown 1974), the central source and its circumnuclear material has been the subject of intense study from infrared to radio frequencies using both continuum and spectroscopic probes.

In the radio continuum, the central few parsecs show a spiral-like structure of thermal emission, termed the minispiral or Sgr A West, roughly centered on the bright, non-thermal point source Sgr A\* (Ekers et al. 1983; Lo and Claussen 1983). The arms of the radio minispiral are interpreted as the ionized remains of tidally-disrupted in-falling clouds, a notion supported by the large ( $\sim 500 \text{ km s}^{-1}$ ) velocity dispersion in the ionized gas observed via mid-IR fine structure and radio recombination lines (Lacy et al. 1980; Schwarz, Bregman & van Gorkom 1989). The distribution of molecular and neutral atomic gas shows a different morphology – interferometric observations of HCN show a substantial portion of an inclined ring-like structure of diameter approximately 3 pc surrounding Sgr A\*, with kinematic evidence for rotational motion of about  $110 \text{ km s}^{-1}$  around the center (Güsten et al. 1987; Wright, Marr & Backer 1989). In contrast, the neutral oxygen emission shows a peak inside the circumnuclear ring, but also shows general evidence of rotational motion in the same sense as the HCN. (Jackson et al. 1993, henceforth J93).

The first far-IR observations demonstrated that the substantial IR luminosity (few  $\times 10^6 L_{\odot}$ ) at the center of the galaxy is due to dust absorbing UV and optical energy and

reradiating it at longer wavelengths (Hoffman, Frederick & Emery 1971; Gatley et al. 1977; Gatley & Becklin 1981). Subsequent mapping revealed bi-lobal structure with temperature decreasing with distance from the center, suggesting a circumnuclear ring or disk around a central 2–3 pc evacuated cavity containing the primary luminosity source (Becklin, Gatley & Werner 1982).

The far-IR, radio continuum, and molecular features have been unified with high-resolution far-IR images (Latvakoski et al. 1999). Far infrared images at 31 and 38  $\mu\text{m}$  provide color temperature, optical depth, and luminosity maps of the inner  $2 \times 3$  pc region, and trace the deposition of UV luminosity and constrain the masses of the features. The most prominent feature is the CND itself. Here the far-IR typically peaks 1–3'' (0.03–0.1 pc) further from Sgr A\* than the radio continuum (e.g. Sgr A West), and the molecular gas ring as traced with HCN has a larger radius still. This is as would be expected in a typical photodissociation region (PDR) situation in which the progression from the UV source is: ionized gas traced with radio continuum—photodissociated gas and warm dust—molecular gas. Given the similarity in the morphology and kinematics of the the radio arcs, the far-IR ring, and the HCN ring, a plausible scenario is therefore that these features trace different aspects of the same structure, a ring or torus of material orbiting the central mass, called the circumnuclear disk (CND).

In addition to the CND, the other other prominent features distinctly traced in both the far-IR and radio are the Northern Arm (NA) and the east-west bar; both part of the radio source identified as SGR A West. The radio continuum and far-IR morphologies again make a nice match, and their kinematics as probed via the radio recombination lines suggests that these features are distinct infalling streamers on parabolic orbits around Sgr A\*. The neutral oxygen emission ([OI]) was originally attributed to material within the cavity formed by the CND (J93), but has been shown to be primarily originating from the NA itself. The sizes and column densities as traced with the dust continuum imply average gas densities of  $1.6\text{--}4 \times 10^4 \text{ cm}^{-3}$ , consistent with the average densities derived for the atomic gas ( $10^4\text{--}10^5 \text{ cm}^{-3}$ ).

Aside from a few local heating sources, the color temperature map of the region presented by L93 is strongly peaked in the center near Sgr A\*, and the run of temperature with radius follows the same  $T \sim r^{-0.4}$  law across all of the features. The central cluster massive young He I stars centered within an arcsecond of Sgr A\* (collectively called IRS 16), in concert with the other stellar clusters thus makes an appealing mechanism for centrally ionizing and heating the material in the CND and the other streamers (L99).

While the UV sources near Sgr A\* are thus a good explanation for the warm dust and atomic gas in the NA, and the inner edge of the CND, UV photons are not necessarily the heating source of the molecular material that comprises the bulk of the CND. Various

theoretical models for the formation of the CND invoke infalling clouds and require cloud-to-cloud collisions (Vollmer & Duschl 2002; Sanders 1998). Dynamical heating has been suggested as a mechanism for molecular clouds in the Galaxy’s central 500 pc to explain bright rotational H<sub>2</sub> lines (Rodriguez-Fernandez et al. 2000, 2001) and the presence of highly-excited NH<sub>3</sub> (Wilson et al. 1982; Herrnstein & Ho 2002). At the position of Sgr A\* itself, the ro-vibrational molecular hydrogen lines show an almost completely thermal spectrum, much like the Orion-KL shock (Tanaka et al. 1989; Gatley et al. 1986), demonstrating that UV is not responsible for the heating of this warm molecular gas.

Thus, the question remains open: what are the relative roles of the dynamical and ultraviolet energy sources in exciting the molecular gas in the central 2 cpc? More generally, what is the origin, lifetime, and eventual fate of this material? To address these questions, we have mapped the J=7→6 rotational transition of carbon monoxide (CO) in this region. The mid-J CO rotational transitions are especially useful probes for the Galactic Center because they are thermalized and optically thick in the circumnuclear disk, but suffer little extinction and virtually no line optical depth in the foreground Galactic material. We use CO lines to estimate the mass and conditions of the warm molecular gas. We trace more than 2000M<sub>⊙</sub> and derive a moderate density,  $n \sim 2 - 7 \times 10^4 \text{ cm}^{-3}$ , and warm temperature  $T \sim 200 - 300 \text{ K}$ . Unlike the atomic gas and the warm dust traced in the far-IR continuum, the bulk of this warm molecular component is likely heated dynamically via magneto-hydrodynamic shocks due to clump-clump collisions, not UV photons from the central sources.

The observations are described in Section 2. Section 3 presents the results of our CO observations and a brief comparison with the morphological and kinematic features observed in other tracers. (We will present a more detailed morphological study using a larger, higher-spatial-resolution map in a subsequent article.) Analysis of the CND molecular gas excitation is presented in Section 4, and a discussion of the CND gas heating mechanism follows in Section 5.

## 2. Observations

The CO J=7→6 ( $\nu = 806.65, \text{ GHz}$ ) observations were made in April 1999 at the James Clerk Maxwell Telescope (JCMT) on the commissioning run of the submillimeter Fabry-Perot spectrometer SPIFI. Details of the instrument and its performance can be found in Bradford et al. (2002). In its first-light configuration, the detector array included 12 bolometers, arranged on an incomplete 4×4 grid with 8" spacing. Over the two nights, the array was placed in eleven positions, six of which included sufficient field rotation to warrant being split into two pointings, generating a total of 17 independent pointings of the array. Each

pointing is comprised of 30–50 spectral scans of the Fabry-Perot with the telescope nodded every two scans to exchange the source and reference beams. For these observations, the velocity resolution of the spectrometer was  $70 \text{ km s}^{-1}$ , and the total scan bandwidth was  $620 \text{ km s}^{-1}$ . The spectra were sampled at  $50 \text{ km s}^{-1}$ , but the data are rebinned at a finer resolution to allow proper co-adding of the various pixels around the array, each of which has a small relative velocity shift.

Calibration was based on Mars, which was near opposition and was taken to be a uniform disk of size  $15.8''$  and brightness temperature 201 K, the mean of the models of Wright (1976) and Rudy et al. (1987). At the time of the observations, the forward coupling of the telescope was measured to be 0.65, of which 8.5% coupled to Mars. This low value of the coupling to Mars resulted from a combination of telescope surface and misfigured reimaging lenses. On subsequent observing runs this coupling was measured to be  $\sim 20\%$ , consistent with other observations at 800 GHz.

All Galactic Center observations were conducted in submillimeter band 2 weather ( $\tau_{225} > 0.05$ ). When combined with the low elevation of the source, this provided a transmission to the source between 0.03 and 0.10. The atmospheric transmission for each scan was determined with the 225 GHz radiometer according to

$$\tau_{806 \text{ GHz}} = 37 (\tau_{225 \text{ GHz}} - 0.012). \quad (1)$$

This relation was calibrated by measuring sky emission against an ambient load as a function of zenith angle, and comparing the derived opacity to the measured 225 GHz opacity. With the low telescope coupling and atmospheric transmission, the system NEFD for the observations was  $\sim 3 \times 10^{-21} \text{ erg s}^{-1} \text{ cm}^{-2} \text{ Hz}^{-1} \text{ Hz}^{-\frac{1}{2}}$ .

Once the twelve spectra were generated from each pointing, the total flux for each pixel in each pointing is calculated by integrating over  $-160 \text{ km s}^{-1} < v < 160 \text{ km s}^{-1}$ , to provide adequate baseline, and trace the same gas as with HCN and  $\text{NH}_3$ . The overlaps in the various pointings then allow for determining the appropriate scalings between the various pointings, these relative scalings are as much as a factor of 1.8 over the entire set of 17 pointings, but the scaling does not change by more than 30% between two pointings adjacent in time.

The spectra were then mosaiced together by regridding onto a uniform  $0.43''$  spatial by  $10 \text{ km s}^{-1}$  spectral grid. At a given velocity,  $T_{\text{MB}}$  in each pixel is determined by any surrounding data points as follows: Each observed point is placed into the spatial array as a delta function with magnitude equal to its intensity. The map is generated by smoothing this array with an  $11''$  gaussian kernel, then normalizing each position by a template map obtained by the same smoothing of an array with unity at each data point. With the

incompletely-filled array, and the effects of field rotation some regions of the map are highly sampled, other are very sparse, thus the sensitivity in the map varies substantially. For a typical interior point in the map, there are between one and three spectra per beam, and we estimate the relative uncertainty to be  $\sim 300 \text{ K km s}^{-1}$  from beam to beam, and about twice this value across the entire map, the additional error accumulating due to the mosaicing together of several pointings. The map boundaries are defined to be where the template array drops below 0.4, that is, where there is not a single observed point within  $6''$ , thus large regions near the map boundaries may be influenced only by a small number of observed points. The overall calibration uncertainty is estimated to be about 30%, due to the varying atmospheric conditions during the observations and calibration.

### 3. Results

The integrated intensity map in CO  $J=7 \rightarrow 6$  of the central 2 pc is presented in Figure 1, along with five spectra of various positions offset from Sgr A\*. Emission is observed throughout the  $2' \times 1'$  mapped region, with a minimum integrated intensity of  $900 \text{ K km s}^{-1}$  (referred to the main beam temperature). The peak in the CO emission is in the southwest, likely part of the CNB, with an intensity of  $5400 \text{ K km s}^{-1}$ , and the average intensity throughout the region is  $2550 \text{ K km s}^{-1}$ . In this section we first compare our results with previous observations of the same tracer. We then compare our map with high-resolution maps in the far-IR continuum and the density tracer HCN in order to address the morphology and kinematics of the warm-CO containing gas. Hereafter we adopt a distance of  $7.9 \pm 0.3 \text{ kpc}$  to the Galactic Center, according to the analysis of McNamara et al. (2000).

#### 3.1. Comparison with previous observations

The integrated intensities we measure are somewhat lower than those of Harris et al. (1985), who observed CO  $J = 7 \rightarrow 6$  in nine  $30''$  beams offset in galactic longitude from Sgr A\*. Harris et al. (1985) do not present a two-dimensional map, but their brightest observed position is toward the southwest part of the Circumnuclear Disk (CND) with a total measured luminosity of  $200 L_{\odot}$  in the  $30''$  beam. Integrating over a  $30''$  beam centered on the peak in our map results in only  $105 L_{\odot}$ . A potential explanation for this discrepancy is self-chopping in our observation. We employed a  $120''$  chop in RA, the maximum usable for efficient operation at the JCMT. With this chop the reference beam does approach the “+20  $\text{km s}^{-1}$ ” and “+50  $\text{km s}^{-1}$ ” Sgr A clouds, large extended clouds lying roughly 1–3' to the east of Sgr A\* (Genzel et al. 1990). Genzel et al. (1990) have observed these objects

in CO  $J=7 \rightarrow 6$  with a roughly eight  $30'$  pointings, finding peak intensities around 600–800  $\text{K km s}^{-1}$ , over large ( $\sim 1'$ ) regions. Harris et al. (1985) were able to use a  $190''$  chop throw on the IRTF, which clears the majority of the Sgr A clouds. While the chopping onto these clouds is thus a difference between our observations and those of Harris et al., the effect is not likely to account for the significant difference in observed intensities. Because we were nodding the telescope, exchanging between an eastern and a western reference beam, the error introduced by an  $800 \text{ K km s}^{-1}$  source in one of the reference beams is at most  $\sim 400 \text{ K km s}^{-1}$ , or  $\sim 10\%$  of the observed flux density. Our spectra show no obvious indication of reference beam emission and a comparison of our primary dataset with a small sample dataset obtained using a  $90''$  chop does not show any evidence of reference beam emission affecting the map. Apart from the overall calibration difference, our map corresponds well with the large-beam pointings of Harris et al., both in relative integrated flux, and in velocity spread of the emission across the region.

Moneti, Cernicharo & Pardo (2001) present a single  $J=7 \rightarrow 6$  spectrum toward Sgr A\*, obtained with the CSO, their data show an integrated intensity of  $700 \text{ K km s}^{-1}$  in  $T_A^*$ . Taking a main beam efficiency of 0.3, as in our measurements with the JCMT, this corresponds to a main beam intensity of  $2330 \text{ K km s}^{-1}$ , 64% of the  $3650 \text{ K km s}^{-1}$  we measure. Our measurements are therefore intermediate between the other published values, which vary by a factor of more than two.

### 3.2. Morphology and kinematics

CO  $J=7 \rightarrow 6$  emission is detected throughout our observed region. We reserve the detailed kinematic and morphological study for the higher-spatial-resolution, larger area dataset presented in a subsequent paper. For the purposes of this study, we simply overlay the CO dataset on the  $38 \mu\text{m}$  continuum image (Latvakoski et al. 1999) in Figure 2 and the interferometric HCN map (Güsten et al. 1987) in Figure 3. We highlight two points which lead to the conclusions that the gas tracing the mid-J CO bears some relation but is not identical to the CND material traced with HCN or the high-excitation  $\text{NH}_3$ .

1) The bright CO emission peak in the southwest is coincident with the far-IR peak at the same location:  $(-15, -30)$ . This location corresponds to a smaller radius (1.2 pc projected) but the same position angle as the HCN peak. The bright CO emission  $20\text{--}30''$  south of Sgr A\* is similar to that found in the map of  $\text{NH}_3$  (6,6), tracing molecular gas at a few hundred K (Herrnstein & Ho 2002). We note that with our moderate spatial resolution and relatively small coverage, the CO and  $\text{NH}_3$  maps do not agree in detail, as the  $\text{NH}_3$  peak is further east. In general, both tracers show that warm gas is interior to the circumnuclear

ring as traced with HCN.

2) Kinematically, the warm CO shows evidence of motion about Sgr A\*. The spectra in Figure 1 reveal a clear north-south velocity gradient with the same sense of rotation as is observed in the HCN. However, the CO  $J=7 \rightarrow 6$  does not show the obvious ring shape, nor the well-organized circular orbit of the dense gas traced with the HCN. Neglecting the morphological asymmetry, the observed orbital velocity of  $\sim 60 \text{ km s}^{-1}$  line of sight ( $65 \text{ km s}^{-1}$  deprojected with  $67^\circ$  inclination), at a distance of  $35''$  suggests an interior mass of only  $1.3 \times 10^6 M_\odot$ . This is substantially less than the mass traced with HCN, and dramatically less than the central dark mass traced with the stellar velocity field ( $M \sim 4.0 \times 10^6 M_\odot$  (Ghez et al. 2003; Schödel et al. 2003)). Evidently, the CO-containing gas does not have angular momentum for a stable orbit at its distance from the central mass. Herrnstein & Ho (2002) reached a similar conclusion in their mapping of  $\text{NH}_3$  (6,6). Again aside from this general similarity, the two tracers do not share detailed kinematics: the CO shows a sense of rotation similar to that of the HCN, while the  $\text{NH}_3$  does not. Given

#### 4. Physical conditions in the GC molecular gas

Bright CO  $J=7 \rightarrow 6$  emission implies the presence of both warm and dense gas. The  $J=7$  level lies 155 K above ground and the  $J=7 \rightarrow 6$  transition has a high critical density,  $n_{\text{crit}} = 4 \times 10^5 \text{ cm}^{-3}$  for thermalization. Our peak brightness temperature of 33 K originates in gas with a minimum physical temperature of  $T = \frac{h\nu}{k} [\ln(\frac{h\nu}{kT_{\text{MB}}} + 1)]^{-1} = 51 \text{ K}$ , if the transition were optically thick, thermalized, and filled the  $11''$  beam. This is a strong lower limit – in reality the gas is at lower density and does not fill the beam, which requires a higher temperature.

##### 4.1. LVG radiative transfer calculations

We combine our  $J=7 \rightarrow 6$  observations with published CO observations in the far-IR ( $J=14 \rightarrow 13$  and  $J=16 \rightarrow 15$  (Lugten 1987)) and millimeter ( $J=2 \rightarrow 1$  and  $J=1 \rightarrow 0$  (Serabyn et al. 1986)) to estimate the conditions in the molecular gas in the framework of an LVG radiative transfer model. The code calculates intensities of the rotational CO lines up to  $J=18 \rightarrow 17$ , given a molecular hydrogen density, temperature, and velocity gradient in  $\text{km s}^{-1} \text{ pc}^{-1}$ . The process was originally employed for the study of molecular clouds by Scoville & Solomon (1974) and Goldreich and Kwan (1974), and further description of the model used here can be found in Bradford et al. (2003). As in their study of the nuclear



molecular gas in NGC 253, we adopt a velocity gradient much larger than the traditional values of a few  $\text{km s}^{-1} \text{pc}^{-1}$  appropriate only for cool, quiescent molecular clouds in the disk of the Milky Way. For the material in the central 2 pc, we take  $dv/dz$  to be  $300 \text{ km s}^{-1} \text{pc}^{-1}$ , consistent with our observed velocity width of  $\sim 100 \text{ km s}^{-1}$  in an  $11''$  beam. We adopt  $8 \times 10^{-5}$  for  $X_{\text{CO}}$ , the CO fractional abundance relative to  $\text{H}_2$ . This value is intermediate between that inferred from observations of the massive Galactic clouds Sgr B2 and Orion IRc2 (for which  $X_{\text{CO}} \sim 6 \times 10^{-5}$  (Leung, Herbst and Huebner 1984; Evans, Lacy, & Carr 1991)), and that of chemical models (for which  $X_{\text{CO}} \sim 1.5 \times 10^{-4}$  (e.g. Blake et al. (1987))). Collisional rates are from Flower (2001, 2004), increased by 21% to account for collisions with helium (McKee et al. 1982; Viscuso & Chernoff 1988; Flower & Launay 1985; Schinke et al. 1985).

For a meaningful run of line intensity with  $J$ , all observed intensities are averaged over a  $44''$  beam corresponding to the far-IR beam size. This average beam is centered toward the  $J = 7 \rightarrow 6$  peak in the southwest at  $(-15, -30)$ . Figure 4 shows the constraints imposed by two line ratios. We use the  $J = 16 \rightarrow 15$  to  $J = 7 \rightarrow 6$  and  $J = 7 \rightarrow 6$  to  $J = 2 \rightarrow 1$  ratios, as these straddle the peak in the run of intensity versus  $J$ . The heavy contours correspond to observed ratios, and their intersection region represents the range of possible solutions. With errors on the submillimeter and far-IR intensities estimated at 30%, the line ratios should be considered good to  $\sim 40\%$ , admitting a large range of solutions over which temperature can be traded with density. It is clear that the temperature is greater than 200 K, and that the molecular hydrogen density is less than  $10^5 \text{ cm}^{-3}$ , though there are no stringent upper limits on the temperature using the available rate coefficients. We favor temperatures toward the lower end of the allowed range shown in Figure 4 because of the lack of evidence for higher-temperature molecular tracers, as discussed in Section 4.3). Given this constraint, we plot a suitable solution ( $n_{\text{H}_2} = 7.1 \times 10^4 \text{ cm}^{-3}$ ,  $T = 240 \text{ K}$ ) superposed on the observed line intensities in Figure 5. In this model,  $\tau$  exceeds unity for  $J_{\text{upper}} = 7-10$ , but does not exceed 2 due to the large velocity gradient appropriate in the CND. Our conclusions for the SW CND are inconsistent with the conditions reported by Moneti, Cernicharo & Pardo (2001) for the gas toward Sgr A\* itself:  $T \sim 250 \text{ K}$ , and  $n_{\text{H}_2} \sim 3 \times 10^5 \text{ cm}^{-3}$ . We deduce smaller densities, in spite of using the same collisional rates from Schinke et al. (1985). All of our inferences are based on a fit to the observations toward the peak of the CO emission in the southwest CND. It is possible that the molecular gas is more highly excited toward Sgr A\* itself than in the SW CND, though distinguishing between the two is difficult given the large beams for the high- $J$  far-IR lines. Based on the  $50''$  resolution ISO maps of Sgr A\* in CO  $J = 14 \rightarrow 13$  (White et al. 1998), we estimate that the CO line ratios are similar throughout the region, suggesting similar excitation conditions in the gas. If so, the discrepancy may arise from our large velocity gradient which should be applicable given the dynamics

of the region, which allows the  $J=7$  transition to radiate more efficiently and with lower collisional excitation than in more optically thick models.

## 4.2. Molecular gas mass, clumping

Using the model plotted in Figure 5, the required CO column density is  $N_{\text{CO}} = 1.2 \times 10^{18} \text{ cm}^{-2}$  in the  $44''$  beam, or  $N_{\text{H}_2} = 1.5 \times 10^{22} \text{ cm}^{-2}$  with our assumed CO abundance of  $8 \times 10^{-5}$ . The  $44''$  represents  $2.2 \text{ pc}^2$ , and total molecular gas mass in this beam is therefore  $530 M_{\odot}$ . If the excitation conditions are similar throughout our mapped region, then we can scale the column density with the observed  $J=7 \rightarrow 6$  intensity. In this case, the beam-averaged column density in a beam toward Sgr A\* itself is  $\sim 60\%$  of our peak value, and is 6 times that reported by Moneti, Cernicharo & Pardo (2001). This discrepancy is difficult to reconcile. It could be due in part to the larger CSO beam relative to our JCMT observations, though this effect is unlikely given that our map shows extended emission. More fundamentally, even if the  $J=7 \rightarrow 6$  transition were optically thin and thermalized, it would be impossible to generate the observed emission toward the peak in our map with the CO column density reported by Moneti, Cernicharo & Pardo (2001). On the other hand, our analysis could be consistent with a larger CO column given the lack of any optically thin mid-J CO isotopic transitions. Other analyses of cooler material suggest somewhat larger molecular column densities. For example J93 compile low-J CO, CS, and HCN measurements, and infer  $N_{\text{H}_2} = 4 \times 10^{22} - 4 \times 10^{23} \text{ cm}^{-2}$ , in  $10''$ – $30''$  beams toward the SW CNB. They suggest that the HCN emission comes from very dense ( $n_{\text{H}_2} = 10^6 - 10^8 \text{ cm}^{-3}$ ) material, distributed with low beam filling factor in small clumps. While our analysis indicates that this density is not appropriate for the material which produces the bulk of the mid-J CO emission, it is possible that clumps at these high densities could harbor molecular gas which could be locally optically thick, and thus inefficient in contributing to the total CO emission. Again, we stress that our model employs a higher temperature, and larger velocity gradient, both of which allow the CO to radiate more efficiently than previously considered. Thus our mass and column density estimates should be considered as lower limits to the total warm molecular gas mass. Finally, we note that our analysis is not sensitive to cool gas which does not radiate in the high-J lines, and a cool component could exist along with the warm one we measure. Such a two-component molecular medium (25% at 200 K, 75% at 25 K) has been proposed based on the high-J  $\text{NH}_3$  observations of GC clouds (Huettemesiter et al. 1993; Herrnstein & Ho 2004).

Scaling the mass in the  $44''$  beam to the entire map using the CO  $J=7 \rightarrow 6$ , intensity yields a mass of  $\sim 2 \times 10^3 M_{\odot}$  as a lower limit to the warm molecular gas in the central

2 pc. Comparing the total mass with the derived density implies a volume filling factor of  $4.4 \times 10^{-2}$ , and an area filling factor of 0.12 in the  $44''$  beam. This filling factor is reasonable – it is approximately equal to the product of the filling factor of the overall ring shape as observed at the  $11''$  resolution in the  $44''$  beam used for the calculations, and the intrinsic clumpiness in the ring on scales below our  $11''$  beam. The size of the clumps is not constrained with the large-beam analysis. At a maximum, all of the  $530 M_{\odot}$  of gas is in a single 0.6 pc diameter clump, corresponding to  $A_V = 138$  mag. The facts that we are resolving the ring shape in our  $11''$  beam, and that the HCN and far-IR maps show clumping at the limit of their resolution ( $4\text{--}12'' = 0.15\text{--}0.46$  pc) suggest that material is clumped on smaller scales (L99, Güsten et al. (1987); Wright et al. (2001)). A clump size of order 0.2 pc might be expected on physical grounds, as it is comparable to the Jeans length scale, over which self-gravity becomes important,

$$L_J = \left( \frac{kT}{mG\rho_m} \right)^{\frac{1}{2}} \sim 0.2 \text{ pc} \quad (2)$$

for the cooler conditions inferred from the CO lines,  $T = 200$  K, and  $n_{\text{H}_2} = 7 \times 10^4 \text{ cm}^{-3}$ . With this size, the  $44''$  beam harbors 25 clumps, each with a mass of  $22 M_{\odot}$ , and the clump column density corresponds to  $A_V = 47$ . This is sensible in a scenario in which clumpy molecular material is falling toward Sgr A\* from greater distance, but is not appropriate for a steady-state motion at the distance of the CND. Any clump with density less than  $n_{\text{H}_2} \sim 6 \times 10^7 \text{ cm}^{-3}$  is Roche unstable in the presence of the tidal forces of the central mass concentration. Thus any clumps associated with the material emitting CO are most likely transient structures.

### 4.3. Molecular gas luminosity

The CO excitation model provides a good estimate of the mass and total cooling due to CO in the molecular gas. The above fit to the data corresponds to a total emergent intensity in the CO lines of  $1.5 \times 10^{-2} \text{ erg s}^{-1} \text{ cm}^{-2} \text{ sr}^{-1}$  averaged over the  $44''$  modeled region. This intensity is substantial, comparable to that of the far-IR atomic fine structure lines (see Table 1), and about 0.1% of the integrated dust continuum intensity. The modeled column density corresponds to a mass density of  $7.05 \times 10^{-2} \text{ g cm}^{-2}$ , and assuming that the CO lines radiate isotropically, we derive a mass to luminosity ratio of  $L_{\text{CO}}/M_{\text{H}_2} = 1.4 L_{\odot}/M_{\odot}$  for the CO cooling around Sgr A\*.

For a complete energy budget of the warm molecular gas, we now consider the other coolants. Detailed chemical studies indicate that in addition to CO, the most important cooling paths for densities above  $10^3 \text{ cm}^{-3}$  and temperatures above 150 K are the rotational

transitions of H<sub>2</sub> and H<sub>2</sub>O, and the fine structure lines of atomic oxygen ([O I]) (Goldsmith and Langer 1978; Neufeld, Lepp & Melnick 1995, and references therein). In what follows, we estimate the efficiency of these coolants conclude that for the conditions we derive with our LVG analysis, it is likely that CO, H<sub>2</sub>, and [O I] contribute comparably to the cooling budget.

The quadrupole H<sub>2</sub> lines have low radiative rates and are thus optically thin and thermalized at the our modeled densities. The cooling per gram is then easily estimated using (for details see Le Bourlot, Pineau des Forets, & Flower (1999)):

$$\frac{L}{M} = \sum_J \frac{f_u A_{u,l} h\nu}{1.43 \cdot 2m_p} \quad (3)$$

where  $f_u$  is the fraction in the upper level, given by the Boltzmann's equation and  $\eta_{op}$  is the ortho-to-para ratio. The rotational H<sub>2</sub> lines are thermalized for densities above  $10^4 \text{ cm}^{-3}$ , and combined ortho and para cooling function is not strongly dependent on the  $\eta_{op}$  for  $T > 100 \text{ K}$ . With  $T = 240 \text{ K}$ , and  $\eta_{op} = 3$ , the most important line is the  $J = 3 \rightarrow 1$ , which produces  $0.29 L_\odot/M_\odot$ . All of the H<sub>2</sub> lines combined generate  $\sim 0.41 L_\odot/M_\odot$  at this temperature, some 30% of the CO cooling. We do note that the H<sub>2</sub> lines become much more efficient coolants as the temperature increases. For  $T = 325 \text{ K}$ , the H<sub>2</sub> line cooling becomes comparable to our measured CO cooling, and any moderate density ( $n < 10^6 \text{ cm}^{-3}$ ), high temperature regions will be cooled primarily by the H<sub>2</sub> lines.

As the density increases, the oxygen-bearing species O, O<sub>2</sub>, and H<sub>2</sub>O become important. Because the oxygen elemental abundance ( $\sim 3 \times 10^{-4}$ ) is larger than that of carbon ( $\sim 1.4 \times 10^{-4}$ ) (Savage & Sternbach 1996), there is atomic and molecular oxygen in the UV-shielded cloud interiors where all the gas-phase carbon is locked up in CO. The chemical models for warm molecular gas (e.g. Neufeld, Lepp & Melnick (1995)) predict a O<sup>0</sup> and O<sub>2</sub> abundances relative to H<sub>2</sub> of  $1 \times 10^{-4}$  (each) for  $T < 250 \text{ K}$ . As the temperature increases to  $\sim 500 \text{ K}$ , all of the oxygen not locked in CO is likely in the form of H<sub>2</sub>O; its contribution is described below. Since O<sub>2</sub> is not an important coolant due to its lack of a strong dipole, we only need to consider the fine structure transitions of [OI], and of the two, only the  $J = 1 \rightarrow 0$   $63 \mu\text{m}$  is energetically important. The upper level of the  $63 \mu\text{m}$  transition lies 228 K above ground, and would thus would be well-populated given the temperature in the molecular gas if not for the high density required to thermalize the transition,  $n_{\text{crit}} = 8 \times 10^5 \left(\frac{100}{T[\text{K}]}\right)^{0.69} \text{ cm}^{-3} = 4.4 \times 10^5 \text{ cm}^{-3}$ . Neglecting the upper (J=0) level, we can model an emergent intensity under a two-level approximation:

$$I_{[OI]63\mu\text{m}} \sim \frac{h\nu N_O A}{4\pi} \times \left[ \frac{\frac{g_u}{g_l} e^{-\frac{h\nu}{kT}}}{1 + \frac{g_u}{g_l} e^{-\frac{h\nu}{kT}} + \frac{n_{\text{crit}}}{n}} \right] = 1.0 \times 10^{-2} \text{ erg s}^{-1} \text{ cm}^{-2} \text{ sr}^{-1} \quad (4)$$

where  $g_u$  and  $g_l$  are the statistical weights,  $A = 9 \times 10^{-5} \text{ s}^{-1}$ , and we have taken the temperature and density from the CO analysis. We have assumed that the emission is optically thin, which is reasonable given the large velocity dispersion of the warm molecular gas:

$$\tau = \frac{c^3 AN_O}{8\pi\nu^3 \Delta\nu} \left[ \left(1 + \frac{n_{\text{crit}}}{n}\right) e^{\frac{h\nu}{kT}} - 1 \right] \times \left[ \frac{\frac{g_u}{g_l} e^{-\frac{h\nu}{kT}}}{1 + \frac{g_u}{g_l} e^{-\frac{h\nu}{kT}} + \frac{n_{\text{crit}}}{n}} \right] = .25. \quad (5)$$

Correcting for extinction and averaging the [OI] maps of J93 over the  $44''$  beam toward the SW peak, White et al. (1998) obtain an intensity of  $2.4 \text{ erg s}^{-1} \text{ cm}^{-2} \text{ ster}^{-1}$  (see Section 4.4). In this region, therefore, the neutral oxygen present in the molecular gas produces nearly half of the observed [OI]  $63 \mu\text{m}$  emission, and represents 70% of the total cooling in the CO lines. Evidently the neutral oxygen plays an important role in cooling this warm dense molecular gas, and much of the observed [OI] should be attributed to the molecular phase, not the atomic gas.

For very warm molecular gas  $T > 300 \text{ K}$ ,  $\text{H}_2\text{O}$  becomes an important molecular coolant. Chemical models predict a  $\text{H}_2\text{O}$  abundance relative to  $\text{H}_2$  as high as  $3 \times 10^{-4}$  as the temperatures increases to  $500 \text{ K}$ , as it is the dominant oxygen repository under these conditions. Once formed through the chemical network, there are several far-IR rotational transitions of  $\text{H}_2\text{O}$ , and their radiative rates are fast because of the molecule's large dipole moment. For densities sufficient to thermalize these transitions, they will therefore dominate the cooling of the gas. The critical densities, however, are of order a few  $\times 10^5 \text{ cm}^{-3}$ , larger than the density inferred with the CO lines. For the gas we observe, both the temperature and the density of the gas are thus insufficient to generate and excite  $\text{H}_2\text{O}$  substantially and it is not likely a major contributor to the cooling budget. Recent observations with the Odin satellite confirm that the cooling is small:  $\sim 60 \text{ K km s}^{-1}$  in the  $557 \text{ GHz}$  ( $1_{1,0} \rightarrow 1_{0,1}$ ) in the  $2.1 \text{ arcmin}$  diameter beam (Sandqvist et al. 2003). Taking the warm gas to fill the beam gives a lower limit to the intensity of  $1.1 \times 10^{-5} \text{ erg s}^{-1} \text{ cm}^{-2} \text{ sr}^{-1}$ , about 80 times less than the CO  $J=7 \rightarrow 6$  line. If all this flux is referred to the  $44''$  beam used in the CO analysis, the integrated intensity would be  $8.3 \times 10^{-5} \text{ cm}^{-3}$ , this represents a generous upper limit, but is still 10 times smaller than the observed CO  $J=7 \rightarrow 6$  line. Furthermore, shorter wavelength  $\text{H}_2\text{O}$  lines observed with the ISO-LWS are only found in absorption from foreground

cold gas in the continuum – none of the profiles show evidence for emission with intensities comparable to the CO lines (Moneti, Cernicharo & Pardo 2001), and are therefore rule out a large amount of gas with temperatures higher than  $T \sim 250$  K.

The theoretical modeling and the observational evidence therefore support the following cooling budget for the warm molecular gas if it is at the modeled temperature and density: the CO lines account for half of the total cooling, the [OI] 63  $\mu\text{m}$  line one third, and the H<sub>2</sub> rotational lines one sixth. The total corresponds to a mass-to-luminosity ratio of  $2.7 L_{\odot}/M_{\odot}$ . As discussed above, for any material at higher temperatures the H<sub>2</sub> and H<sub>2</sub>O lines will become more efficient at cooling the gas, and the total cooling of the molecular gas will substantially increase.

#### 4.4. Relationship with the atomic gas

In order to understand the relationship between the atomic and molecular ISM phases, it is necessary to distinguish between the morphological features in the central 2 pc. Estimates of the mass of atomic gas by J93 were based on their model fits to the [OI] and [CII] intensities toward the peak 25'' north east of Sgr A\*. Most of this emission is now believed to come from the northern arm (NA), a tidally-stretched infalling streamer that is dynamically distinct from the rest of the circumnuclear material (L99, citetryg96). The dust optical depth in the NA corresponds to a hydrogen column density of  $N_{\text{H}} \sim 0.7\text{--}1.3 \times 10^{22} \text{ cm}^{-3}$  (in the 4''–6'' far-IR beams), corresponding to an ultraviolet attenuation of only 2–4 magnitudes through the streamer, insufficient to shield the bulk of the material from photodissociation. This optical depth, together with the proximity to the UV sources makes the NA the dominant feature in the atomic tracers, but it is negligible in the overall mass budget of the molecular material in the central 2 pc.

By comparison, the dust emission toward the molecular peaks in the SW CND is associated with cooler, but much more massive structures. The optical depths in the clumps in the ring are an order of magnitude greater than in the northern arm, in general sufficient to shield the UV from the bulk of the material. As discussed in Section 4.3, the warm molecular material as probed with the CO emission is responsible for much of the [OI] emission observed toward the SW ring. The other half arises in the atomic component. To estimate the atomic gas mass fraction, we use the [OI] map to scale the mass estimate of J93 for the NA to the atomic fraction in the SW CND peak. Including the extinction correction for J93, they estimate  $N_{\text{H}} = 1.2 \times 10^{22} \text{ cm}^{-2}$  based on an intensity of  $5.0 \times 10^{-2} \text{ erg s}^{-1} \text{ cm}^{-2} \text{ sr}^{-1}$  (22'' beam). The  $\sim 2.0 \times 10^{-2} \text{ erg s}^{-1} \text{ cm}^{-2} \text{ sr}^{-1}$  observed in the 44'' multiplied by 0.5 to remove the molecular gas component then scales to an atomic gas column of  $N_{\text{H,SW atomic}} \sim 2.4 \times 10^{21} \text{ cm}^{-2}$ .

Taking this SW peak as indicative of the rest of the overall region, we conclude that the atomic gas makes a small contribution to the total mass:  $\sim 8\%$  of that of the warm molecular material.

A plausible scenario is that the molecular and atomic gas are physically associated and coexist as different phases in the same morphological structures (e.g. clumps in the ring), as has been proposed by Genzel et al. (1985) and J93. For clumps illuminated from one side (as for a centrally-heated region centered on Sgr A\*), the fraction of photodissociated material is estimated by the ratio of the extinction in a typical PDR layer ( $A_{V,\text{PDR}} \sim 4$ ) to the extinction through the full clump. The fiducial 0.2 pc clumps / streamers discussed above would have  $A_V = 47$ ; thus for such structures, the mass ratio of the photodissociated surface layer to the bulk is consistent with the mass ratio based on the intensities.

## 5. Heating of the Molecular Gas

Having estimated the conditions and total cooling of the molecular gas in the Galaxy’s central 2 pc, we turn now to its heating source. There are two potential mechanisms: photoelectric heating by UV photons, and dynamical heating. Both are a priori plausible near Sgr A\*, given its intense UV sources and turbulent dynamical structure. Morphological evidence suggests that UV heating may be important. Warm CO peaks interior to the HCN ring in general, and at the same position as the far-IR emission in the southwest ring. The emission observed toward the north of Sgr A\* may also be associated with the NA as it enters the cavity. Furthermore, the emission in [SiII], [CII] and the far-IR continuum requires UV heating, and the maps in these tracers are generally well-explained in the context of  $\sim 10^7 L_\odot$  of visible-UV luminosity, most from near Sgr A\*, illuminating dense clumps and streamers (L99).

However, a scenario that *only* involves UV photons exciting the molecular gas is difficult to support quantitatively. The intensity of the CO J=7→6 transition relative to the atomic lines and far-IR continuum is much larger than can be accounted for with any existing PDR model. The standard plane-parallel PDR models (Tielens & Hollenbach 1985; Kaufman et al. 1999) predict mid-*J* CO emission arising from a layer between  $A_V \sim 3$  and  $A_V \sim 7$ : at  $A_V \lesssim 3$  CO is photodissociated, and at  $A_V \gtrsim 7$  the UV does not produce the heating necessary to excite these transitions. These models predict a [OI] 63  $\mu\text{m}$  / CO J=7→6 ratio,  $R$ , between 600–1200 (Kaufman et al. 1999), nearly two orders of magnitude higher than our observed  $R \sim 15$ . The Orion Bar PDR presents a similar problem to the theory, though not as extreme, with  $R \sim 130$  (Stacey et al. 1993). Clumpy models have been generated in attempts to explain the discrepancy (Burton et al. 1990; Meixner & Tielens 1993; Koster

et al. 1994), and Burton et al. find that the Orion PDR intensities can be reasonably well-modeled (to within factors of two) as a mixture of clumpy PDRs, including some clumps with very high densities ( $n = 10^7 \text{ cm}^{-3}$ ). Unlike in the Orion PDR, however, a model which incorporates a large fraction of the gas at high density is not supported for Sgr A\*, given the drop off in CO line intensity above  $J \sim 10$ . The best clumpy PDR model of Burton et al. for Sgr A\* based on the atomic lines, CO lines, and molecular hydrogen lines underestimates the CO  $J=7 \rightarrow 6$  line intensity by a factor of 25. The root of the problem is the fact that there is  $\sim 15$  times more warm molecular gas than atomic gas, geometrically impossible for UV-heated medium. On this basis we rule out UV heating as a viable method for all but a small fraction of the warm molecular gas we observe. Rodriguez-Fernandez et al. (2001); Rodriguez-Fernandez et al. (2004) reach a similar conclusion in their study of  $\text{H}_2$  rotational line emission from other Galactic Center clouds.

### 5.1. Shock Conditions in the Central 2 pc

We conclude that dissipation of supersonic turbulence in shocks is a more likely source for heating the warm molecular material in the central 2 pc. Dynamical heating has been proposed in explaining the emission from rotational  $\text{H}_2$  lines in Galactic Center clouds Rodriguez-Fernandez et al. (2004), and the presence of SiO in these clouds suggest a chemical history which includes shocks (Huettemeister et al. 1998). Various models for the origin and dynamics of the features around Sgr A\* have been constructed (Vollmer & Duschl 2002; Sanders 1998, e.g.), which include infalling clouds and clump-clump collisions. The presence of clumps which are not Roche stable in the CNB supports the notion that molecular material feeds into the central parsecs, and that dynamical effects are important. Observations of molecular hydrogen provide further evidence – the molecular hydrogen ro-vibrational lines observed toward the northeast and southwest CNB show a spectrum which is almost completely thermal, very much like the Orion shock (Tanaka et al. 1989; Gatley et al. 1986). Qualitatively, the spectral tracers around Sgr A\* show some similarity to the shock region in Orion (BN-KL), with very bright CO lines relative to all other tracers, [OI], [CII], and the continuum (see Table 1). As indicated by the high-J lines, however, the shock conditions in the bulk of the GC gas are clearly less intense than the Orion KL shock, where the CO emission is modeled to arise in the warm gas downstream of the  $38 \text{ km s}^{-1}$  shock.

To derive the shock conditions, we invoke the magnetohydrodynamic C-shock models of Draine, Roberge, & Dalgarno (1983, hereafter DRD), Draine & Roberge (1984), and Roberge & Draine (1990). These models span a large parameter space—density, velocity, and magnetic field all affect the post-shock conditions. When applied to the GC region, the



difficulty is the potentially large magnetic field. DRD present CO intensities only for models with standard magnetic field,  $B = 100 \mu\text{G} \left(\frac{n}{10^4 \text{cm}^{-3}}\right)^{0.5}$ . The field strength has a tremendous impact of the post-shock excitation, in general the peak temperature is proportional to the square of the magnetic field and square of the shock velocity. An increase in the field strength by a factor of 3 can reduce high- $J$  line intensities as much as a factor of 100, while the peak  $J$  and its intensity remain approximately unchanged. Other high-excitation lines such as those of  $\text{H}_2\text{O}$ ,  $\text{H}_2$ , and  $[\text{OI}]$  are similarly affected. The direct observational constraints on the field strength are not strong because the Zeeman measurements are difficult. It is known that within 3–4 pc of Sgr A\* there are regions with  $B$  as large as 3 mG, though this does not pervade the region. In the CNB itself, for example, there is no measurable field with an upper limit of 0.5 mG (Plante, Lo, & Crutcher 1995; Marshall, Lasenby, & Yusef-Zadeh 1995). As these investigators point out, however, that the large turbulent and orbital motions may distort and reverse the field such that the average measured field in a large (44") beam may underestimate its local strength.

Using the published low-magnetic-field models, the general shape of the CO line intensity distribution, the peaking at  $J \sim 8$ , and the falling-off toward higher  $J$  is reproduced for a range of density and velocity, from  $n_{\text{H}} \sim 10^4 \text{cm}^{-3}$ ,  $v = 20 \text{km s}^{-1}$  to  $n_{\text{H}} \sim 10^5 \text{cm}^{-3}$ ,  $v = 13 \text{km s}^{-1}$ . In all of these models cases, however, the transitions below the peak ( $\sim J = 1-5$ ) are predicted to be brighter relative to the mid and high- $J$  transitions than is observed. This is likely due in part to the lower- $J$  lines being optically thin in the our observed region due to the large velocity dispersion, relative to the models in which all of the lower- $J$  CO lines are optically thick. A similar effect has been noted in considering the ground-state ( $J = 1 \rightarrow 0$ ) HCN transition emission observed the CNB. The large velocity dispersion produces a low optical depth and reduces self-absorption, producing a high intensity per gas mass as compared with the more typical molecular clouds with less motion (see e.g. Wright et al. (2001)). Given this optical depth consideration, the higher density, lower velocity solution best reproduces the relative CO intensities, underpredicting the  $J = 8/J = 3$  intensity ratio by a factor of only 2. Large magnetic fields are appealing because they allow a great deal of energy to be radiated in a fairly low-excitation gas, this is the sort of situation that is required to reproduce CO luminosity that is comparable to or greater than the luminosity in  $[\text{OI}]$ . Given the CO lines, the observed and inferred  $[\text{OI}]$  intensity, and the published models of DRD, we conclude that a model with density of  $10^4-10^5 \text{cm}^{-3}$ , and velocity-magnetic field product of  $10-20 \text{km s}^{-1} \times 0.5-0.3 \text{mG}$  is the most likely description of the shock conditions in the central 2 pc.

In this scenario, the shock conditions which are exciting the mid- $J$  CO are not likely the same as those which excite the near-IR  $\text{H}_2$  lines. Gatley et al. (1986) have mapped a two-lobe structure in the  $\text{H}_2 \nu = 1 \rightarrow 0 S(1)$  around Sgr A\*, which is consistent with the shape of the CNB, and as pointed out above this emission has been found to be due to

shock excitation (Tanaka et al. 1989). However, the low-velocity C-shocks which account for the observed CO emission would not include appreciable luminosity in the near-IR H<sub>2</sub> lines. These scenarios are not inconsistent; there are likely a variety of shock conditions around Sgr A\*. Gatley et al. (1986) claim that the H<sub>2</sub> emission is due to shocks at the inner edge of the molecular disk due to mass outflow from Sgr A\*. The CO emitting shocks, on the other hand, arise from the dissipation of dynamical turbulence in the bulk of molecular ring.

## 5.2. Turbulent Dissipation and Orbit Decay in the Central 2 pc

We now turn to the energetics of the turbulent dissipation. Stone, Ostriker, & Gammie (1998); Mac Low (1999, and references therein) have studied the dissipation rate in magneto-hydrodynamic (MHD) turbulence, and find that the rate is comparable to that of a pure hydrodynamical turbulence, and is essentially given by dimensional analysis. To get the correct coefficient, we rearrange Equation 7 in Mac Low (1999) to express the energy output per mass of turbulent material as:

$$\frac{L}{M} = 0.42 \frac{v_{\text{rms}}^3}{\Lambda_d} = 1.10 \left( \frac{v_{\text{rms}}}{25 \text{ km s}^{-1}} \right)^3 \left( \frac{1 \text{ pc}}{\Lambda_d} \right) \frac{L_{\odot}}{M_{\odot}}, \quad (6)$$

where  $v_{\text{rms}}$  is the typical turbulent velocity, and  $\Lambda_d$  is the size scale of the typical turbulent structures. The turbulent size scale should be comparable to or smaller than the smallest observed clump size, of order 0.1 pc according to the interferometric HCN measurements (also comparable to the Jeans length scale). We therefore adopt  $\Lambda_d \sim 0.1 \text{ pc}$ . Taking a mid-range value from the above analysis, we apply  $v_{\text{rms}} = 15 \text{ km s}^{-1}$  to Eq. (6), yielding a power dissipated per unit mass of  $(L/M)_{\text{turb}} = 2.4$  in solar units. This is a reasonable match to the observed and inferred cooling rates in CO, [OI], and H<sub>2</sub>. Note also that the adopted values for  $\Lambda_d$  and  $v_{\text{rms}}$  are broadly consistent with the  $300 \text{ km s}^{-1} \text{ pc}^{-1}$  velocity gradient used in the LVG analysis:  $15 \text{ km s}^{-1} / 0.1 \text{ pc} \sim 150 \text{ km s}^{-1} \text{ pc}^{-1}$ .

If the luminosity in the molecular lines is the result of turbulence in the steady state, then the orbit of the molecular material must be decaying. Differentiating the expression for Keplerian motion gives:

$$\frac{dR}{dt} = \frac{2R^2}{GM} \cdot \frac{dE}{dt}, \quad (7)$$

where  $M$  is the enclosed mass and  $E$  represents the energy of per mass of the molecular gas. For an orbit around  $4 \times 10^6 M_{\odot}$  at a distance of 1.5 pc, the observed luminosity to mass ratio corresponds to an orbit decay rate of  $4 \times 10^{-6} \text{ pc yr}^{-1}$ . Thus infall from the radius of

the HCN ring ( $R \sim 2$  pc) to the inner edge of the CND as traced in the far-IR ( $R \sim 1.5$  pc) would require  $1.2 \times 10^5$  yr, similar to the orbital timescale  $\sim 9 \times 10^4$  yr. Thus this gas is dissipating its orbital energy on a orbit timescale, and cannot exist for more than a few orbits, or a few  $\times 10^5$  yr. This is not surprising if the material which forms the CND and other features derives from orbits with low angular momentum, and the CND itself represents the circularization of that material at a radius appropriate for its angular momentum.

Recent modeling has given some theoretical basis for the formation of the CND and streamers as the result of infalling clouds. Sanders (1998) produce an asymmetric elliptical structure, called a dispersion ring, by tidal disruption of a clumpy cloud incident on a point mass from 6.5 pc with angular momentum of a 1 pc radius circular orbit. After the material makes one or two passes (about  $8 \times 10^5$  yr), the resulting debris is a circumnuclear structure which reproduces the kinematics of the HCN ring more accurately than any circular rotation scenario, and hints at the same morphological structure. Though the overall distribution is not symmetric, the innermost edge of the dispersion ring is elliptical, and consistent with the observed far-IR morphology (Latvakoski et al. 1999). Throughout the simulation, the interior radius of the CND gradually decreases, the result of repeated collisions between clumps, which would certainly produce shocks and possibly trigger star formation. Whether the inner radius stabilizes, or some of the gas eventually accretes onto the central mass depends on the details of the viscosity and the formation of stars. Sanders (1998) use a very similar infalling cloud scenario to model the northern arm and the east-west bar, each indendently. This is appealing, as there is convincing observational evidence that the northern arm is an infalling streamer produced in a collision between two clouds somewhere outside the CND (Latvakoski et al. 1999; Herter et al. 1989; Jackson et al. 1993). The northern arm is in an earlier stage of infall than the CND gas, roughly on its first passage, and has lower specific angular momentum, both of which which make it more recognizable observationally. It is significant that the same model can generate the CND morphology and kinematics as traced with the far-IR and the HCN, and provide a natural fit with the dynamically-driven energetics we derive for the material around Sgr A\*.

## 6. Conclusions

We present an  $11''$  spatial resolution map of the central 2 pc of the galaxy in the  $J=7 \rightarrow 6$  rotational transition of CO. An LVG analysis invoking all the available CO line intensities provides constraints on the conditions in the molecular gas. We find that warm, 200–300 K, moderate density,  $n \sim 5\text{--}7 \times 10^4 \text{ cm}^{-3}$ , molecular gas is abundant in the Galactic Center, with total CO luminosity comparable to that of the atomic lines. The total mass of warm

molecular material is at least  $2000 M_{\odot}$ , slightly less than the total mass measured with cooler molecular gas tracers, but an order of magnitude more than the mass in photodissociated atomic gas. Morphologically and kinematically, the CO emission bears some resemblance to the CND as traced with HCN and the far-IR continuum. Heating with a central UV source is not capable of producing the observed CO luminosity, and we conclude that the primary energy source is dynamical. The observed spectral tracers are consistent with mechanical energy being dissipated into the gas in low-velocity ( $10\text{--}20 \text{ km s}^{-1}$ ) shocks with magnetic fields of  $0.3\text{--}0.5 \text{ mG}$ , and these values are consistent with other observational evidence. Our results support a scenario in which the CND and other features around Sgr A\* are each in the process of forming from infalling molecular clouds with low angular momentum on timescales of  $10^5$  years.

We thank Wayne Holland (currently at the UK ATC), Richard Prestage (currently at NRAO Green Bank), and the JCMT operators and technical staff for their help in making the commissioning run of SPIFI a success. We thank David Flower (Durham University) for providing the high-temperature CO-H<sub>2</sub> rate coefficients in advance of publication. C.M.B. acknowledges support from a Milliken Fellowship at Caltech. We thank an anonymous referee for several helpful comments on a draft of the manuscript.

## REFERENCES

- Balick, B., and Brown, R.L. 1974, ApJ, 194, 265
- Becklin, E.E. & Neugebauer, G. 1968, ApJ151, 145
- Becklin, E.E. & Neugebauer, G. 1969, ApJ157, L31
- Becklin, E.E., Gatley, I., & Werner, M.W. 1982, ApJ, 258, 135
- Blake, G.A., Sutton, E.C., Masson, C.R., and Phillips, T.G. 1987, ApJ, 315, 621
- Bradford, C.M., Stacey, G.J. Swain, M.R., Nikola, T., Bolatto, A.D., Jackson, J.M., Savage, M.L., and Davidson, J.A. 2002, Applied Optics 41, 2561
- Bradford, C.M., Stacey, G.J., Nikola, T., Bolatto, A.D., Jackson, J.M., Savage, M.L., and Davidson, J.A. 2003, ApJ, 586, 861
- Burton, M.G., Hollenbach, D.J., and Tielens, A.G.G.M. 1990, ApJ, 365, 620
- Draine, B.T. and Roberge, W.G. 1984, ApJ, 282, 491
- Draine, B.T., Roberge, W.G. and Dalgarno, A. 1983, ApJ, 264, 485
- Ekers, R.D., van Gorkom, J.H., Schwarz, U.J. & Goss, W.M. 1983, *a*, 122, 143
- Evans, N.J., Lacy, J.H., and Carr, J.S. 1991, ApJ, 383, 674
- Flower, D.R., and Launay, J.M. 1985, MNRAS, 214, 271
- Flower, D.R. 2001, J. Phys. B, 34, 2731.
- Flower, D.R. 2004, *personal communication*
- Gatley, I., Becklin, E.E. Werner, M.W., & Wynn-Williams, C.G. 1977, ApJ, 216, 277
- Gatley, I. and Becklin, E.E. 1981, in *IAU Symposium 94, Infrared Astronomy*, ed C.G. Wynn-Williams and D.P. Cruikshank (Dordrecht: Reidel), P. 281
- Gately, I., Jones, T.J., Hyland, A.R., Wade, R., Geballe, T.R., & Krisciunas, K. 1986, MNRAS, 222, 299.
- Genzel, R., Pichon, C., Eckart, A., Gerhard, O.E., and Ott, T. 2000, MNRAS, 317, 348.
- Genzel, R., Watson, D.M., Crawford, M.K. and Townes, C.H. 1985, ApJ, 297, 766

- Genzel, R., Stacey, G.J., Harris, A.I., Townes, C.H., Geis, N., Graf, U.U., Poglitsch, A., & Stutzki, J. 1990, *ApJ*, 356, 160
- Ghez, A., Salim, S., Hornstein, S.D., Tanner, A., Morris, M., Becklin, E.E., & Duchene, G. 2003, *astroph/0306130*
- Goldreich, P., and Kwan, J. 1974, *ApJ*, 189, 441
- Goldsmith, P. and Langer, W.D. 1978, *ApJ*, 222, 881
- Güsten, R., Genzel, R., Wright, M.C.H., Jaffe, D.T., Stutzki, J., & Harris, A. 1987, *ApJ*, 318, 124
- Güsten, R. and Wright, M.C.H., 2000, personal communication
- Harris, A.I., Jaffe, D.T., Silber, M., & Genzel, R. 1985, *ApJ*, 294, L93
- Herrmann, F., Madden, S.C., Nikola, T., Poglitsch, A., Timmermann, R., Geis, N., Townes, C.H., Stacey, G.J. 1997, *ApJ*, 481, 343
- Herrnstein, R., and Ho, P.T.P. 2004, *ApJ*, in press, (*astro/ph 0409271*)
- Herrnstein, R. and Ho, P.T.P. 2002, *ApJ*, 579, L83
- Herter, T., Gull, G.E., Megeath, S.T., Rowlands, N., and Houck, J.R. 1989, *ApJ*, 343, 696
- Hoffman, W.R., Frederick, C.L., & Emery R.J. 1971, *ApJ*, 170, L89
- Huettemeister, S., Wilson, T.L., Bania, T.M., and Martin-Pintado, J. 1993, *A&A*, 280, 255
- Huettemeister, S., Dahmen, G., Mauersberger, R., Henkel, C., Wilson, T.L., and Martin-Pintado, J. 1998, *A&A*, 334, 646
- Jackson, J.M., Geis, N., Genzel, R., Harris, A.I., Madden, S., Poglitsch, A., Stacey, G.J., Townes, C.H. 1993, *ApJ*, 402, 173
- Kaufman, M.J., Wolfire, M.G., Hollenbach, D.J., Luhman, M.L. 1999, *ApJ*, 527, 795
- Koster, B., Storzer, H., Stutzki, J., & Sternberg, A. 1994, *A&A*, 284, 558
- Lacy, J.H., Townes, C.H., Geballe, T.R., Hollenbach, D.J. 1980, *ApJ*, 241, 132
- Latvakoski, H.M., Stacey, G.J., Gull, G.E., Hayward, T.L. 1999, *ApJ*, 511, 761
- Le Bourlot, J., Pineau des Forets, G., and Flower, D.D.R., 1999, *MNRAS*, 802

- Lo, K.Y., and Claussen, M.J. 1983, *Nature*, 306, 647
- Leung, C.M., Herbst, E., and Huebner, W.F. 1984, *ApJS*, 56, 231
- Lugten, J.B. 1987, Ph.D. Thesis, University of California, Berkeley, CA
- Mac Low, M.-M. 1998, *ApJ*, 524, 169
- Marshall, J., Lasenby, A.N., and Yusef-Zadeh, F. 1995, *MNRAS*, 274, 519
- McKee, C.F., Storey, J.W.V., Watson, D.M., and Green, S. 1982, *ApJ*, 259, 647
- McNamara, D.H., Madsen, J.B., Barnes, J., & Ericksen, B.F. 2000, *PASP*, 112, 202M
- Meixner, M., and Tielens, A.G.G.M. 1993, *ApJ*, 405, 216
- Moneti, A., Cernicharo, J., and Pardo, J.R., 2001, *ApJ*, 549, L203.
- Neufeld, D.A., Lepp, S., and Melnick, G.J. 1995, *ApJS*100, 132
- Oort, J.H. and Rougoor, G.W. 1960, *MNRAS*, 121, 171
- Plante, R.L., Lo, K.Y., and Crutcher, R.M. 1995, *ApJ*, 445, L113
- Roberge, W.G. and Draine, B.T. 1990, *ApJ*, 350, 700
- Roberts, D.A., Yusef-Zadeh, F., and Goss, W.M. 1996, *ApJ*, 459, 627
- Rodríguez-Fernández, N.J., Martín-Pintado, J., de Vicente, P., Fuente, A., Hüttemeister, S, Wilson, T.L., and Kunze, D. 2001, *A&A*, 365, 174
- Rodríguez-Fernández, N.J., Martín-Pintado, J., Fuente, A., de Vicente, P., Wilson, T.L., and Hüttemeister, S. 2001, *A&A*, 365, 174
- Rodríguez-Fernández, N.J., Martín-Pintado, J., Fuente, A., Wilson, T.L., 2004, *A&A*, in press,
- Rudy, D.J., Muhleman, D.O., Berge, G.L., Jakosky, B.M., & Christensen, P.R. 1987, *Icarus*, 71, 159
- Sanders, R.H. 1998, *MNRAS*, 294, 35
- Sandqvist, Aa. et al. 2003, *A&A*, 402, L63
- Savage, B.D., & Sternbach, K.R. 1996, *ARA&A*, 34, 279

- Schmid-Burgk, J., Densing, R., Krugel, E., Nett, H., Roser, H.P., Schafer, F., Schwaab, G., van der Wal, P. & Wattenbach, R., 1989, *A&A*, 215, 150
- Schinke, R., Engel, V., Buck, U., Meyer, H., and Diercksen, G.H.F. 1985, *ApJ*, 299, 939
- Schödel R., Ott, T., Genzel, R., Eckart, A., Mouawad, N., & Alexander, T. 2003, *ApJ*, 596, 1015
- Schwarz, U.J., Bregman, J.D. & van Gorkom, J.H. 1989, *å*, 215, 33
- Scoville, N.Z., and Solomon, P.M. 1974, *ApJ*, 187, L67
- Serabyn, E., Güsten, R., Walmsley, C.M., Wink, J.E., and Zylka, R. 1986, *A&A*, 169, 85
- Stacey, G.J., Jaffe, D., Geis, N., Genzel, R., Harris, A., Poglitsch, A., & Townes, C.H., 1993, *ApJ*, 404, 219
- Stone, J.M., Ostriker, E.C., & Gammie, C.F. 1998, *ApJ*, 508, L99
- Sutton, E.C., Danchi, W.C., Jaminet, P.A., and Masson, C.R. 1990, *ApJ*, 348, 503
- Tanaka, M., Hasegawa, T., Hayashi, S., Brand, P.W.J.L., and Gatley, I. 1989, *ApJ*, 336, 207
- Tielens, A.G.G.M., & Hollenbach, D., 1985, *ApJ*, 291, 722
- Viscuso, P.J. and Chernoff, D.F. 1988, *ApJ*, 327, 364
- Vollmer, B., and Duschl, W.J. 2002, *å*, 128
- White, G.J., Smith, H.A., Stacey, G.J., Fischer, J., Spinoglio, L., Baluteau, J.-P., Cernicharo, J., Bradford, C.M. 1998, in *Proceedings of The Universe as seen by ISO*, P. Cox, M.F. Kessler, eds., p. 787
- Wilson, T.L., Ruf, K, Walmsley,C.M., Martin,R.N., Batrla,W., and Pauls,T.A. 1982, *A&A*, 115, 185
- Wright, E.L. 1976, *ApJ*, 210, 250
- Wright, M.C.H., Marr, J.M. and Backer, D.C. 1989, HCO<sup>+</sup> and HCN Observations of SGR a, in *IAU Symp. 136: The Center of the Galaxy*
- Wright, M.C.H., Coil, A., McGary, R.S., Ho, P.T.H., and Harris, A.I. 2001, *ApJ*, 254, 268.



Table 1. Galactic Center ISM tracers

	Sgr A* <sup>a</sup>	Galactic Center		Orion OMC 1	
		N. Arm (25'') <sup>b</sup>	SW CND (25'') <sup>b</sup>	Bar PDR <sup>c</sup>	KL Shock <sup>c</sup>
OI 63 $\mu\text{m}$	$2.1 \times 10^{-2}$	$4.1 \times 10^{-2}$	$2.3 \times 10^{-2}$	$4.0 \times 10^{-2}$	$2.7 \times 10^{-2}$
OI 145 $\mu\text{m}$	$8. \times 10^{-4}$	(1)	(0.93)	$3.5 \times 10^{-3}$	$3.0 \times 10^{-3}$
CII 158 $\mu\text{m}$	$1.7 \times 10^{-3}$	(1)	(1)	$4.2 \times 10^{-3}$	$3.5 \times 10^{-3}$
CI 609 $\mu\text{m}$	$4. \times 10^{-5}$				
CO $J=1 \rightarrow 0$		— $7. \times 10^{-7}$ —		$4. \times 10^{-7}$	$2.7 \times 10^{-6}$
CO $J=7 \rightarrow 6$	$8 \times 10^{-4}$	$1.1 \times 10^{-3}$	$1.5 \times 10^{-3}$	$3 \times 10^{-4}$	$9 \times 10^{-3}$
CO $J=14 \rightarrow 13$	$1.7 \times 10^{-4}$			$3.1 \times 10^{-4}$	$8.6 \times 10^{-3}$
Far-IR cont.	22	50	26	26	390
Ratios					

<sup>a</sup>Intensity ( $\text{erg s}^{-1} \text{cm}^{-2} \text{sr}^{-1}$ ) averaged over a  $2'$  diameter beam around Sgr A\*. The far-IR line intensities are taken from Jackson et al. (1993); Genzel et al. (1985), the CO  $J=7 \rightarrow 6$  from this work, and the CO  $J=1 \rightarrow 0$  from Serabyn et al. (1986). The far-IR continuum is from the luminosity maps of Latvakoski et al. (1999), and includes a contribution of 30% from the warm transiently heated dust grains which are not traced by the 32–38  $\mu\text{m}$  continuum. All intensities are corrected for extinction toward the galactic center, for which we take  $\tau = 23.5 \lambda[\mu\text{m}]$  after Latvakoski et al..

<sup>b</sup>Average intensities over 25'' beams, for tracers with sufficient angular resolution, units and references as above. Relative intensities in the two regions for tracers with larger ( $\sim 1'$ ) beams are given in parentheses, estimated from the ISO LWS maps of White et al. (1998). (RA, Dec) Offsets from Sgr A\*: N. Arm, (+5'', +15''); SW CND, (–15'', –30'').

<sup>c</sup>Intensities in  $\sim 1'$  regions centered on the far-IR bar, and the BN-KL object of Orion. References are Herrmann et al. (1997); ?; Schmid-Burgk et al. (1989); Stacey et al. (1993); ?.

Fig. 1.— Integrated intensity map of the CO  $J = 7 \rightarrow 6$  emission from the Galactic Center Circumnuclear Disk (CND). Offsets are relative to Sgr A\* ( $RA_{1950} = 17^h 42^m 29^s.3$ ,  $decl_{1950} = -28^\circ 59' 19''$ ), and the beam size is  $11''$  FWHM. Emission is observed throughout the the map; contours are linear in  $T_{MB}\Delta v$ , with a  $250 \text{ K km s}^{-1}$  interval. The peak in the southwest CND is  $5400 \text{ K km s}^{-1}$ , the minimum at the edges of the map is  $750 \text{ K km s}^{-1}$ . Velocity resolution in the spectra is  $70 \text{ km s}^{-1}$ . Overall rotational motion is evident in the shifting of the velocity from north to south.

Fig. 2.— CO  $J=7\rightarrow 6$  contours overlay the greyscale far-IR continuum image of Latvakoski et al. (1999), which shows the morphological features around Sgr A\*. The southwest peak in CO is coincident with the far-IR peak in the southwest CND, while the CO ridge to the north lies between the Northern Arm and the northwest CND. The extension of the Northern Arm to the north is clearly detected in CO. CO contours are in units of  $T_{MB}\Delta v$ , peaking at  $5400 \text{ K km s}^{-1}$ , with interval  $375 \text{ K km s}^{-1}$ .

Fig. 3.— CO  $J = 7 \rightarrow 6$  contours overlay the greyscale interferometric HCN  $J = 1 \rightarrow 0$  map (Güsten & Wright 2000). CO generally peaks interior to the HCN, but shows the same clumpy structure in the northern CND. The gap in the HCN ring to the north corresponds to the extension of the northern arm as traced in CO. CO contours are as in Figure 2.

Fig. 4.— LVG constraints for the gas in the CND. Two line ratios are plotted:  $J = 7 \rightarrow 6$  to  $J = 2 \rightarrow 1$  (solid lines) and  $J = 7 \rightarrow 6$  to  $J = 16 \rightarrow 15$  (dashed lines). Heavy lines correspond to observed values in the SW CND, the two medium-weight lines for each ratio show the range allowed by the 40% uncertainty. Calculations assume a velocity gradient of  $300 \text{ km s}^{-1} \text{ pc}^{-1}$  (see text), and the temperature range reflects the availability of CO-H<sub>2</sub> collisional rate coefficients.

Fig. 5.— Model of the excitation and radiative transfer of CO using a large-velocity-gradient, escape-probability approximation. Observed intensities are averaged over a  $44''$  beam centered at ( $\delta \text{ RA} = -15''$ ,  $\delta \text{ Dec} = -30''$ ) from Sgr A\*. CO  $J = 7 \rightarrow 6$  is from this work, the other points from Lugten (1987); Serabyn et al. (1986); Sutton et al. (1990). Error bars are conservative at 30%, reasonable for the calibration uncertainties in the submillimeter and far-IR lines, but likely an overestimate of the uncertainty in the lower-J lines. The lighter curves demonstrate intensities that would be generated in LTE and without including the effects of radiative excitations of the upper levels.

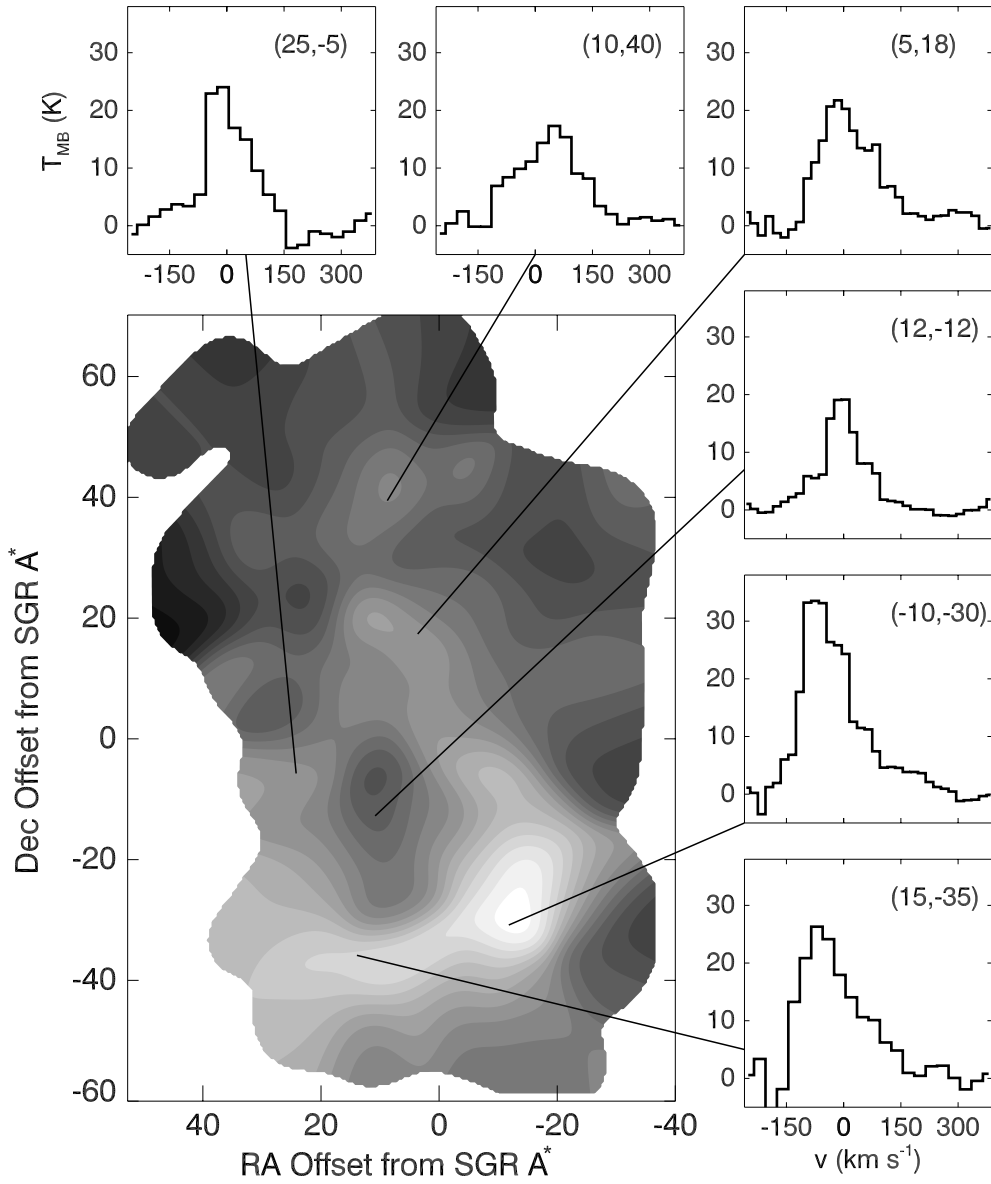


Figure 1, Bradford et al.

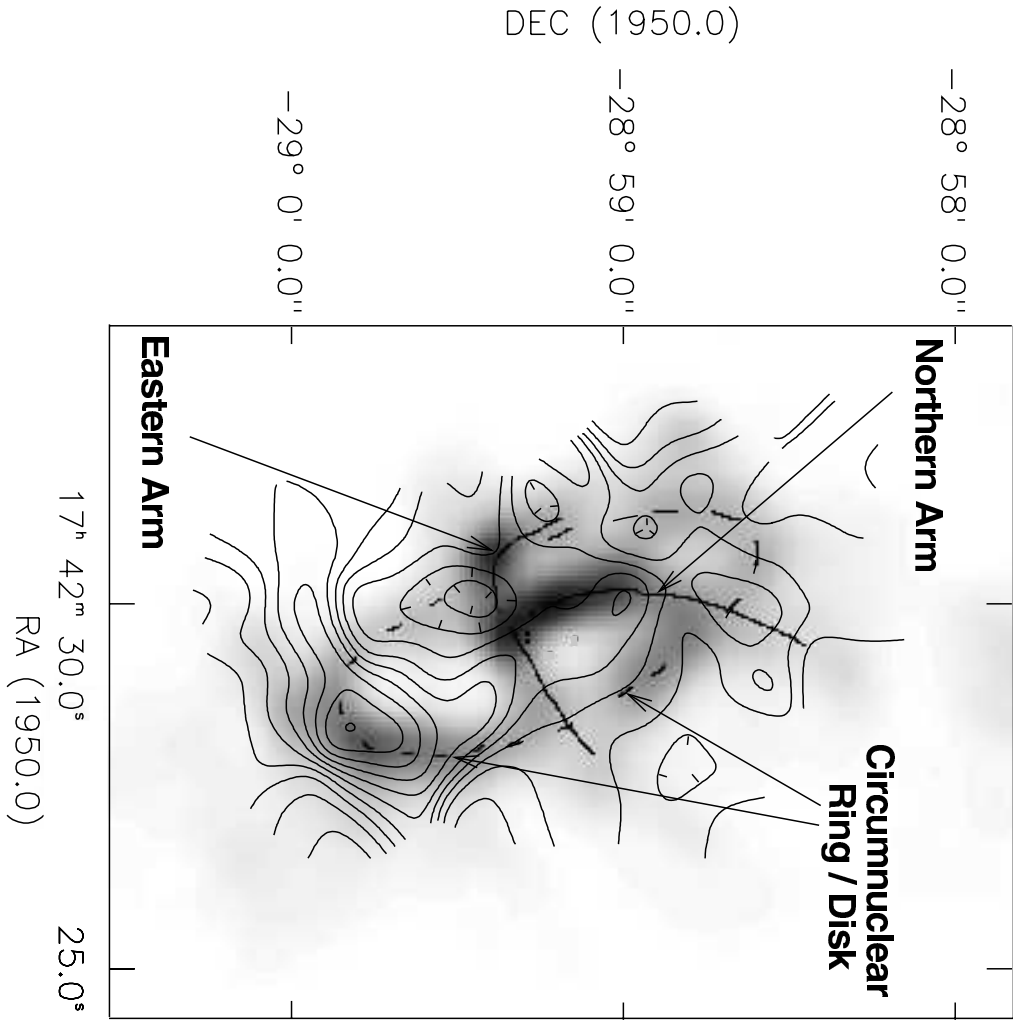


Figure 2, Bradford et al.

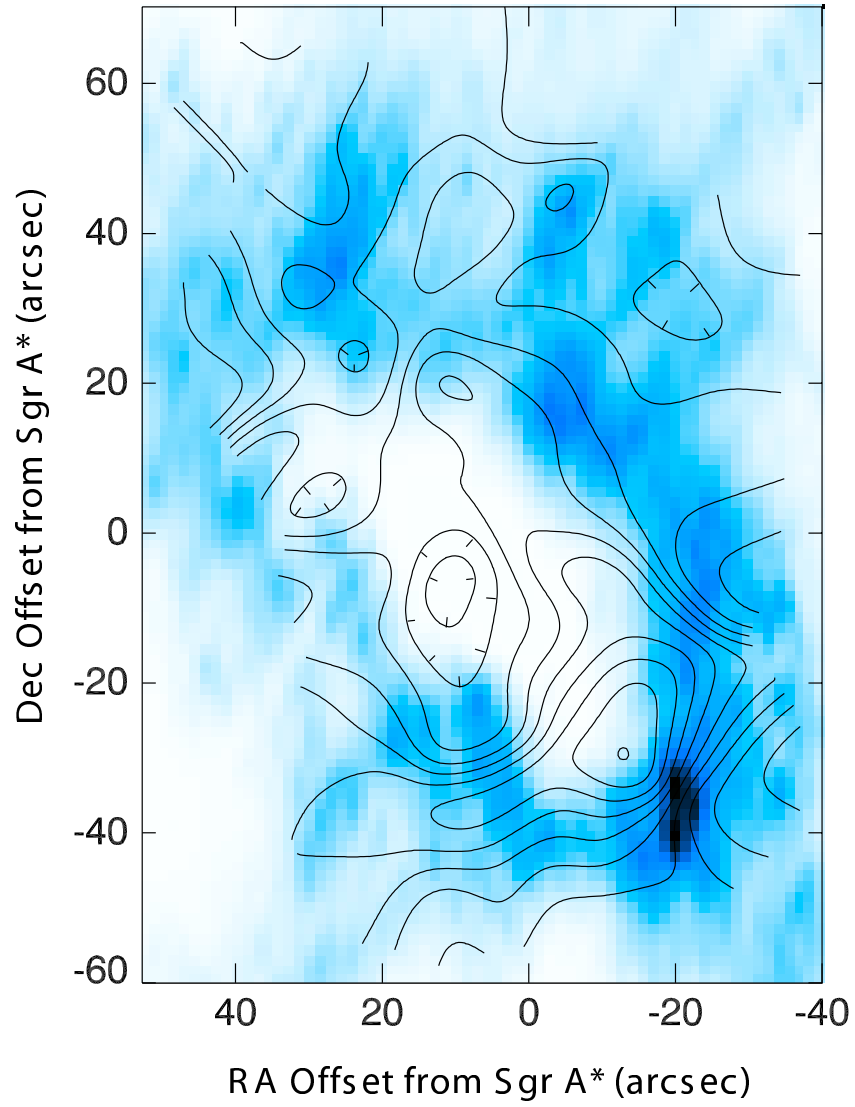


Figure 3, Bradford et al.

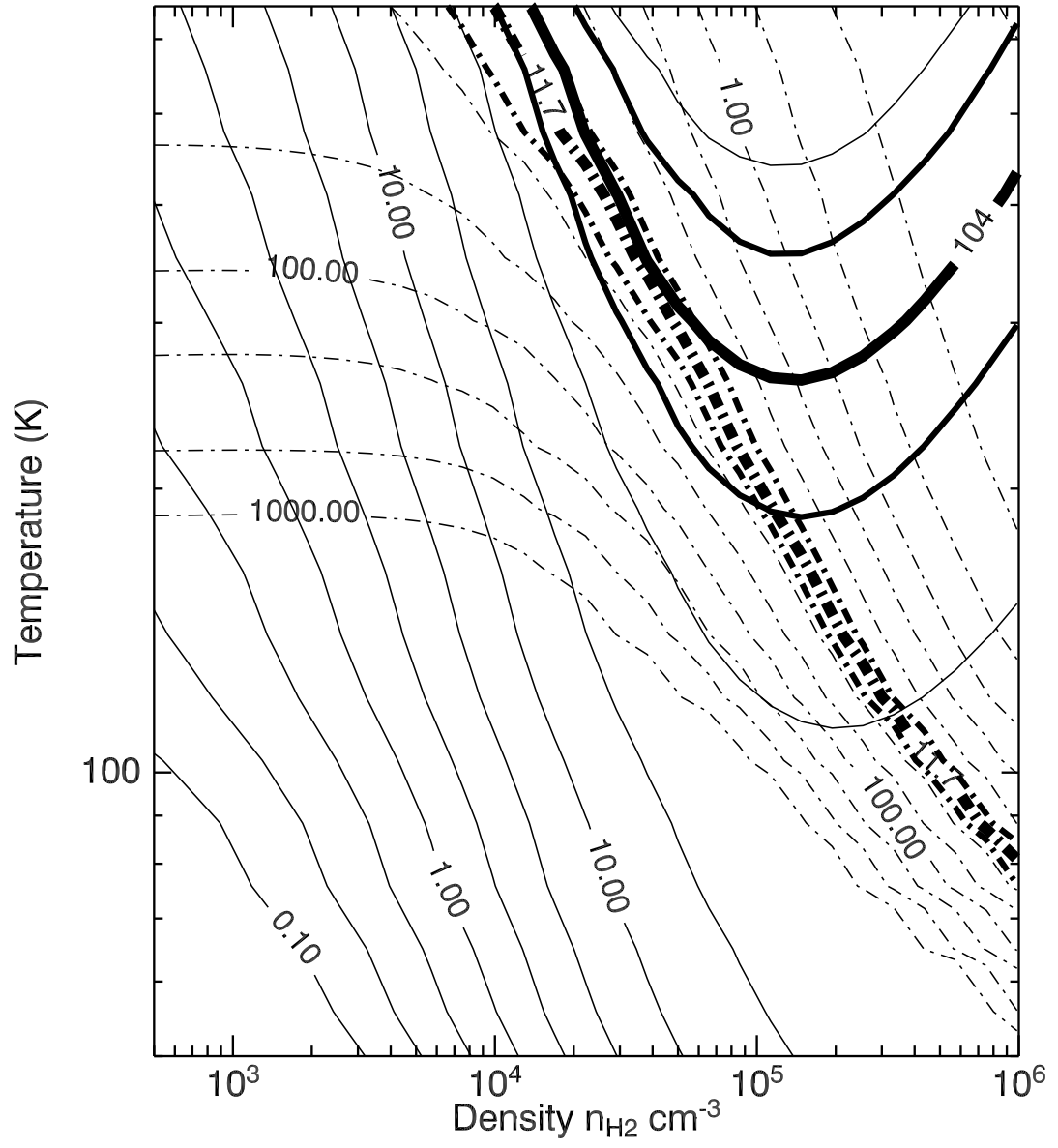


Figure 4, Bradford et al.

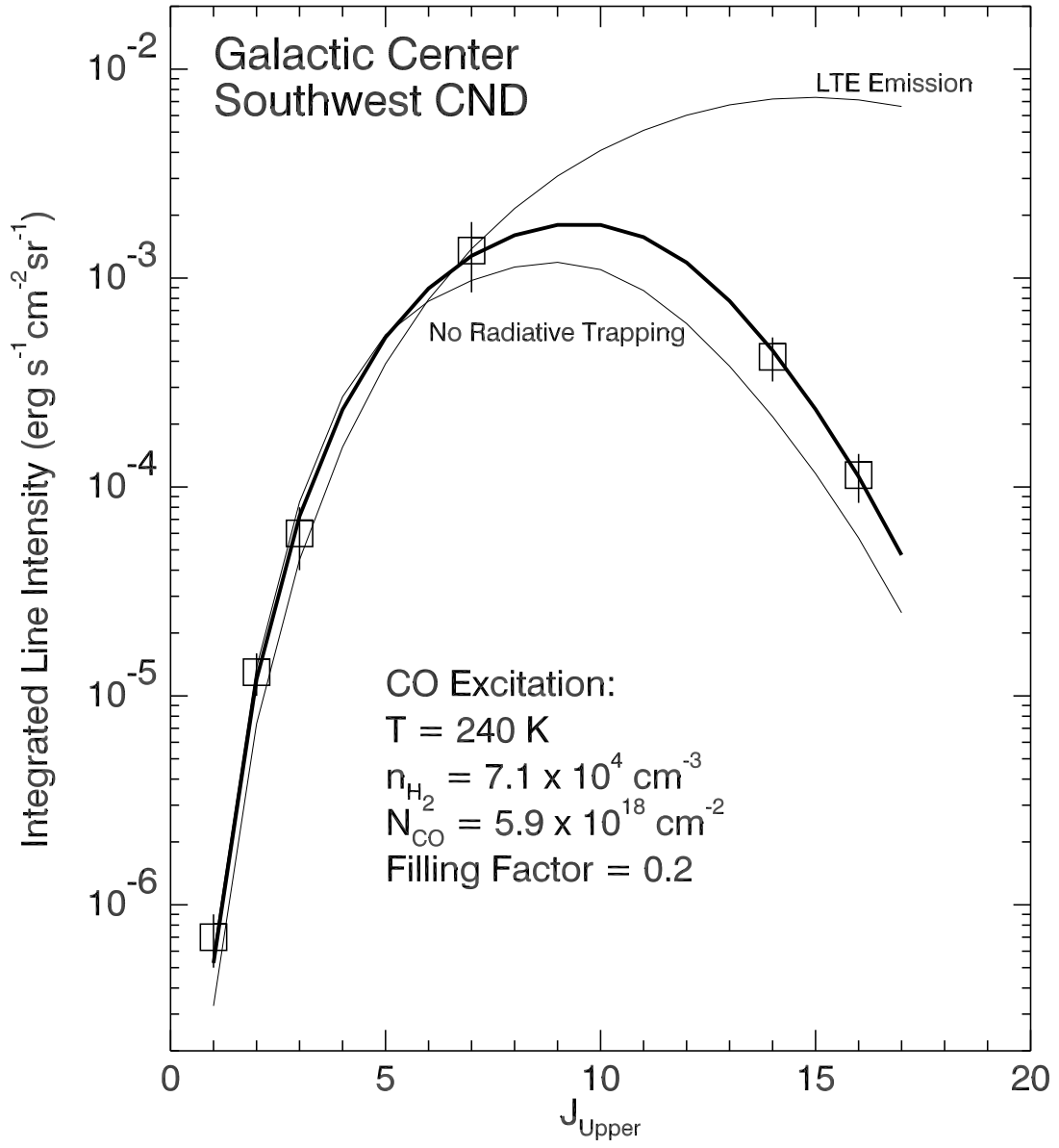


Figure 5, Bradford et al.